Volume 57(4): 289–300, 2009
Journal of Histochemistry & Cytochemistry
http://www.jhc.org

ARTICLE

Assessment of Apoptosis by Immunohistochemistry to Active Caspase-3, Active Caspase-7, or Cleaved PARP in Monolayer Cells and Spheroid and Subcutaneous Xenografts of Human Carcinoma

Aude Bressenot, Sophie Marchal, Lina Bezdetnaya, Julie Garrier, François Guillemin, and François Plénat

Service d'Anatomie et de Cytologie Pathologiques, Hôpital de Brabois, Centre Hospitalier Régional et Universitaire Nancy, Vandoeuvre-lès-Nancy, France (AB,FP), and Centre de Recherche en Automatique de Nancy-Centre National de la Recherche Scientifique Unité Mixte de Recherche 7039 Nancy Université, Centre Alexis Vautrin, Vandoeuvre-lès-Nancy, France (SM,LB,JG,FG)

SUMMARY Immunohistochemistry to active caspase-3, recently recommended for apoptosis detection, is inappropriate to detect apoptosis involving caspase-7. Cleavage of poly-ADP-ribose polymerase 1 (PARP-1), a major substrate of both caspases, is a valuable marker of apoptosis. Apoptosis evaluation induced in vitro either by paclitaxel or by photodynamic treatment (PDT) with Foscan in HT29 or KB monolayer cells and HT29 spheroids yielded a close percentage of labeled cells whatever the antibody used, whereas in control specimens, cleaved PARP (c-PARP) immunostaining failed to detect apoptosis as efficiently as active caspase-3 or -7 immunostaining. Studies in MDA-MB231 monolayer cells and HT29 xenografts either subjected or not subjected to Foscan-PDT resulted in a significant higher number of active caspase-3–labeled cells, although immunofluorescence analysis showed c-PARP and active caspase-3 perfectly colocalized in tumors. A restricted expression of c-PARP was obvious in the greater part of caspase-3 expressing cells from control tumor, whereas photosensitized tumors showed a higher number of cells expressing large fluorescent spots from both active caspase-3 and c-PARP. These results support the assumption that c-PARP expression was dependent on treatment-induced apoptosis. The absence of caspase-7 activation in some caspase-3–expressing cells undergoing Foscan-PDT shows the relevance of using antibodies that can discriminate caspase-dependent apoptotic pathways. **(J Histochem Cytochem 57:289–300, 2009)**

KEY WORDS
apoptosis
caspase-3
caspase-7
poly-ADP-ribose polymerase

THE MOLECULAR and biochemical events of apoptotic cell death have been extensively studied (reviewed in Jin and El-Deiry 2005). Many anticancer drugs induce apoptosis by molecular mechanisms mediated through mitochondrial dysfunction (Green and Kroemer 2004). Release of cytochrome c from the internal part of the mitochondrial membrane into the cytosol results in the activation of caspase cascades, in particular caspase-9, -3, -6, and -7. Because caspase-3 is the main executioner of apoptosis, IHC to the active form of caspase-3 (active casp-3) has been run to check apoptosis in paraffin sections from various tissue (Gown and Willingham 2002; Duan et al. 2003; Resendes et al. 2004; Jakob et al. 2008) and has been recommended in clinical trials as a biomarker of photodynamic treatment (PDT) activity in vivo (Miller et al. 2007). However, it is important to note that apoptosis may also occur through an activation of other executioner caspases such as caspase-7 that could be activated through a mechanism independent of the mitochondrial pathway (Davidson et al. 2005; Pyrko et al. 2007). Moreover, caspase-7 could partially substitute caspase-3 in caspase-3–deficient cells (Mooney et al. 2002; Lakhani et al. 2006). Many protein targets of active caspases are biologically important apoptotic indicators of morphological and biochemical changes associated with apoptosis (Degterev et al. 2003). One of the essential substrates cleaved by both caspase-3 and -7 is poly-ADP-ribose polymerase (PARP), an abundant DNA-binding enzyme that detects and signals DNA strand breaks (Decker and Muller 2002).

Correspondence to: F. Plénat, Service d'Anatomie et de Cytologie Pathologiques, CHU de Brabois, Allée du Morvan, 54511 Vandoeuvre-lès-Nancy, France. E-mail: f.plénat@chu-nancy.fr

Received for publication June 11, 2008; accepted November 6, 2008 [DOI: 10.1369/jhc.2008.952044].

0022-1554/08/$3.30

The presence of cleaved PARP-1 is one of the most used diagnostic tools for the detection of apoptosis in many cell types. The cleavage of PARP-1 into two fragments of 89 and 24 kDa has been considered indicative of functional caspase activation (Koh et al. 2005). However, in sections from ethanol-fixed tissues, specific antibody to cleaved PARP-1 (c-PARP) was unsuccessfully tested (Holubec et al. 2005).

In this study, we assessed apoptosis by using polyclonal antibodies to active caspase-3, active caspase-7, and c-PARP to give a precise insight into the relevance of each marker for the IHC detection of apoptosis. Moreover, the accuracy of antibodies to active caspase-7 and c-PARP to detect apoptosis in histopathology has never been reported in formaldehyde-fixed tissues. Apoptosis was induced in vitro by paclitaxel (McGrogan et al. 2008) or PDT with Foscan (Marchal et al. 2005) in monolayer HT29, KB, and MDA-MB231 carcinoma cell lines or spheroids growing HT29 cells. For the in vivo experiments, we used xenografted HT29 tumors in nude mice that were subjected to Foscan-PDT.

Materials and Methods

Monolayer Cell Cultures

HT29 is a human colon adenocarcinoma cell line, MDA-MB231 is a human mammary adenocarcinoma cell line, and KB is a human cell line related to HeLa cells. These cells were obtained from the American Type Culture Collection (Rockville, MD) and were grown in RPMI-1640 medium (Invitrogen; Cergy-Pontoise, France) without phenol red and glutamine, supplemented with 10% heat-inactivated FCS (PAN Biotech; Aidenbach, Germany), 1% penicillin (10,000 UI/ml)-streptomycin (10,000 μg/ml), and 1% 200 mM glutamine (Invitrogen). Cells were kept at 37C in a 95% air/5% CO_2 humidified atmosphere. They were subcultured every 7 days using 2.5% trypsin with 1 mM EDTA (Invitrogen).

Spheroid Cell Culture

Multicell spheroids of the HT29 cell line were initiated as previously described (Marchal et al. 2005). Briefly, 5×10^4 HT29 cells were seeded into 75-cm^2 flasks previously coated with 1% L-agarose. After 3 days, aggregates were transferred to 250-ml spinner flasks (Integra Biosciences; Chur, Switzerland) containing 150 ml culture medium. The flasks were placed on magnetic plates (Integra Biosciences) at 75 rpm in 5% CO_2 and 37C humidified atmosphere for 15 days. Spheroids reaching ~500 μm in diameter were used in experiments.

Xenografted Tumors

Studies were performed using female athymic Swiss *Foxn*^{1nu}/*Foxn*^{1nu} mice (Harlan; Gannat, France). All animal experiments were carried out in compliance with the French Animal Scientific Procedures Act (April 1988). Mice were housed in plastic cages under standard conditions (25C, 50% relative humidity, 12-hr light/dark cycle) and provided with food and water ad libitum. Procedure to induce HT29 tumors in nude mice was performed as previously described (Coutier et al. 2002). Briefly, 0.1 ml of 8×10^7 HT29 cells/ml in 5% glucose solution was inoculated subcutaneously into the right hind foot. The mice were treated 15 days later when the tumors reached 5 mm in diameter. Three control tumors and seven treated tumors were sampled.

For each treatment (paclitaxel and photodynamic), three experiments were performed on cell lines and cell spheroids. Induction of apoptosis in cell lines, spheroids, and tumor transplants was carried out according to the following procedure.

Paclitaxel Treatment of Monolayers and Spheroids

Monolayer Cells. For each cell line, 3×10^4 cells/ml were seeded into 75-cm^2 flasks. Forty-eight hours after seeding, paclitaxel (Taxol; Sigma-Aldrich, Saint-Quentin Fallavier, France), dissolved in 95% ethanol (100 μM), was added to the culture medium at a final concentration of 0.1 μM. Treatment was carried out for 48 hr. Control cells were treated with 95% ethanol alone (dilution, 1:1000 v/v).

HT29 Spheroids. Approximately 80 spheroids were collected and seeded in 2 ml supplemented medium containing 0.1 μM paclitaxel for 48 hr. Control spheroids were incubated with supplemented medium containing only ethanol (dilution, 1:1000 v/v).

Photodynamic Treatment

Drug Preparation and Administration. Foscan [meta-tetra(hydroxyphenyl)chlorine] was kindly supplied by Biolitec (Jena, Germany). Foscan stock solution was prepared in methanol. Further dilutions of Foscan were performed in RPMI-1640 supplemented with FCS. Injection in animals was performed with a solution of Foscan diluted in a mixture of ethanol, polyethylene glycol, and water (2:3:5) as recommended by the manufacturer. Mice were injected in the tail vein with 0.3 mg/kg body weight at 24 hr before light exposure.

Monolayer Cells. Four days before treatment, 3×10^4 cells/ml of each cell line were seeded in 60-mm-diameter Petri dishes. Logarithmically growing cells were incubated with 1 μg/ml (1.45 μM) Foscan solution in RPMI supplemented with 2% FCS for 24 hr. After two washes, RPMI supplemented with 10% FCS was added, and cells were irradiated with a 650-nm laser diode at a fluence of 0.03 J/cm^2 delivered at a fluence rate of 1.92 mW/cm^2. Control cells were incubated with Foscan and were not subjected to irra-

diation (drug, no light). Twenty-four hours after PDT, cells were collected by trypsinization, washed, and fixed in 4% formaldehyde (pH 7.4).

HT29 Spheroids. HT29 spheroids were treated according to the method previously published (Marchal et al. 2005). Briefly, after a 24-hr incubation with 4.5 μM Foscan RPMI supplemented with 10% FCS, spheroids were irradiated with a 650-nm laser diode at 5 J/cm^2 delivered at a fluence rate of 10 mW/cm^2. Control spheroids were exposed to Foscan without illumination (drug, no light).

HT29 Xenografted Tumors. Twenty-four hours after Foscan IV injection, tumors were irradiated with a 650-nm diode laser at a fluence of 10 J/cm^2 delivered at a fluence rate of 30 mW/cm^2. Control tumors were subjected to Foscan injection without irradiation (drug, no light). Twenty-four hours after PDT, the mice were sacrificed by anesthetic overdose, and the grafts were surgically removed and sectioned in 3-mm-thick slices before being processed.

Sample Collections and Fixation

Twenty-four hours after treatments, monolayer culture cells, spheroids, and tumor samples were fixed in 4% (m/v) formaldehyde (pH 7.4) for 16 hr. Tumors and pellets of monolayer culture cells and spheroids were routinely processed and embedded in paraffin. Paraffin blocks were used to generate 5-μm-thick hematoxylin and eosin–stained sections. Additional slices of transplants were also snap-frozen in isopentane precooled in liquid nitrogen. For each sample of monolayer cells, ultrastructural control was performed.

Transmission Electron Microscope

Cells were fixed overnight at 4C in 3% glutaraldehyde in 0.1 M sodium cacodylate buffer (pH 7.4) and transferred to 0.1 M phosphate buffer (pH 7.2). The cells were postfixed in 1% osmium tetroxide in S-collidine, dehydrated in graded ethanols, transferred to propylene oxide, and embedded in Epon 812. Semithin sections were stained with 1% methylene blue. The sample was further sectioned into ultrathin slices (75 nm), contrasted with uranyl acetate and lead citrate and observed on a transmission electron microscope (CM10; Philips, Eindhoven, The Netherlands).

c-PARP and Active Caspase-3 and-7 Immunolabeling

IHC detection of apoptosis-related proteins was carried out on 5-μm-thick deparaffinized sections. Before IHC, sections were subjected to heat-induced epitope retrieval by incubation in a 0.01 M sodium citrate solution (pH 6) at 120C for 10 min, followed by a 2-hr cool-down. Primary antibodies were diluted in the following buffer: 0.1 M PBS, 0.3% (m/v) BSA, 0.1% (m/v) sodium azide, 0.06% (m/v) n-ethylmaleimide, and 20% (v/v) glycerol (PAB). Active caspase-3 was detected with a species-unspecific rabbit polyclonal antibody (1:1000 diluted; BD Biosciences, Le Pont-de-Claix, France) that specifically recognize the large fragment (17 kDa) of the active protein but not full-length caspase-3. The large fragment of active caspase-7 (20 kDa) was targeted by a species-unspecific rabbit polyclonal antibody (1:50 diluted) provided by Cell Signaling (Danvers, MA). For c-PARP IHC, sections were incubated in a solution of a rabbit polyclonal antibody (1/25 diluted; Cell Signaling, Danvers, MA). This species-specific antibody detects endogenous levels of the large fragment (89 kDa) of human PARP-1 resulting from cleavage at aspartic acid 214 but does not recognize full-length PARP-1 or other PARP isoforms. All antibodies applied in this study were previously used in Western blot analysis with satisfying results (Marchal et al. 2005,2007). Primary antibodies were applied for 16 hr at 4C. The sections were washed in two changes of PBST (0.1 M phosphate buffer, pH 7.4, 0.1% (v/v) Tween 20) over 10 min and incubated with biotinylated goat anti-rabbit antibody (Dakocytomation; Trappes, France) diluted 1:200 for 1 hr at room temperature. After two PBST washes (for 10 min each), endogenous peroxidase activity was blocked by a 10-min incubation in a 6% hydrogen peroxide solution in distilled water. The slides were washed two times in PBST (for 5 min each time) and incubated in streptavidin-peroxidase (Dakocytomation) diluted 1:150 in PBST for 1 hr at room temperature. After two PBST washes of 5 min, bound peroxidase was identified using the Novared TR system (Abcys; Paris, France). Nuclear counterstaining was performed with 1/2-diluted Harris hematoxylin. Each assay was controlled negatively by processing sections in the absence of primary antibody. Good immunostaining data (i.e., low background staining and good precision) were obtained with three antibodies. False-positive cells were only observed in tissue sections of tumor transplants where endogenous biotin was detected by the streptavidin–biotin system of visualization. However, it was easy to distinguish between positive, negative, and false-positive cells. Tumor cells were never artifactually stained, and false-positive staining was limited to mastocytes in mouse connective tissue around the tumors and in sebaceous glands when present.

Determination of Apoptotic Indices

The number of apoptotic cells present in a section expressed as a fraction of the total number of cells, the so-called apoptotic index, measures an apoptotic state. For the purpose of this study, an activated caspase-3 labeling apoptotic index, an activated caspase-7 labeling apoptotic index, and a c-PARP labeling apoptotic index were calculated. The number of labeled

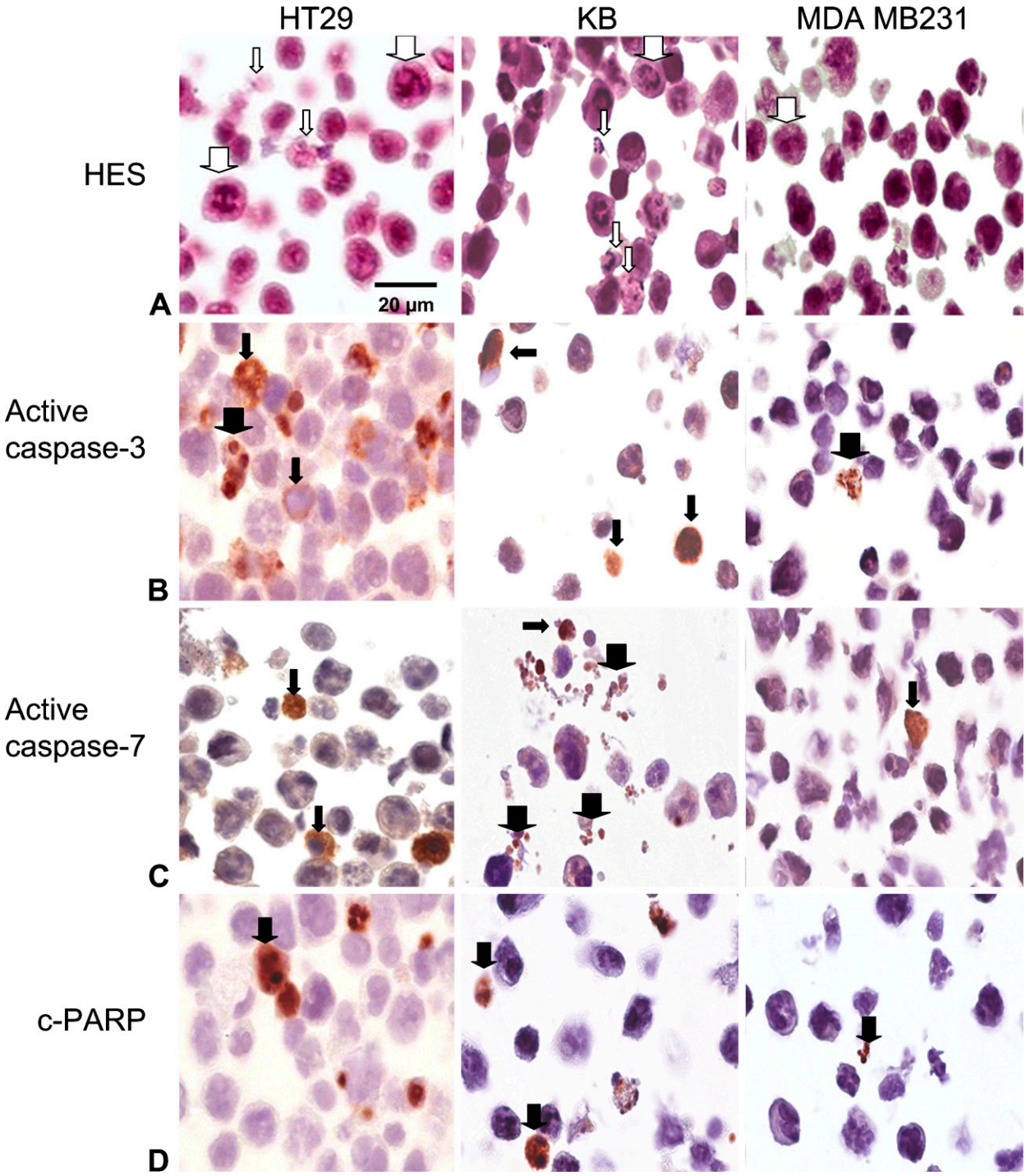

Figure 1 Apoptosis and apoptosis-related protein detection in HT29, KB, and MDA-MB231 monolayer cells subjected to 0.1 µM paclitaxel for 48 hr. (**A**) Paraffin sections were stained with standard coloration hematoxylin-eosin-safran. Note specific morphological features of apoptosis in HT29 and KB monolayers cells (thin white arrows). Numerous mitotic cells were observed in the three cell lines (thick white arrows). (**B**) Active caspase-3 labeling. Note signal cytoplasmic location (thin black arrows) and focally nuclear signal translocation (thick black arrows). (**C**) Active caspase-7 labeling. Cytoplasm location (thin black arrows) and apoptotic bodies (thick black arrows) were observed. (**D**) Cleaved poly-ADP-ribose polymerase (c-PARP) labeling. Nuclear location was noticed (thick black arrows). Harris' hematoxylin counterstain.

cells in immunostained sections were counted relative to 2000 cells in the case of cell pellets. In sections of spheroids, at least three spheroids each composed of >300 non-necrotic cells were considered for each treatment condition. Because the antibody to c-PARP was human specific and did not visualize mouse stromal apoptotic cells, whereas the antisera to active caspase-3 and active caspase-7 stained apoptotic cells in both the stroma and the tumor cell compartment, the apoptotic indices in transplants were calculated as the number of apoptotic cells per total number of epithelial tumor cells. These indices were established by counting at least 2000 cells in fields distant from necrotic areas.

Colocalization Studies

Simultaneous visualization of active caspase-3 and either active caspase- 7 or c-PARP in the same section was carried out in 5-µm-thick frozen sections of two xenografted tumors (one control and one treated). This was achieved by the sequential use of two indirect fluorescence methods whose specificity was previously checked. Active caspase-3 was stained by the first sequence and either active caspase-7 or c-PARP by the second one. Briefly, frozen sections were first fixed with 30% v/v polyethylene glycol in 95C ethanol for 10 min. They were then dried at room temperature for 15 min, washed in absolute ethanol, and rehydrated in PBST for 5 min. They were incubated in a solution of the anti-active caspase-3 rabbit antiserum (1/1000 dilution in PAB for 3 hr at room temperature). The sections were washed twice with PBST for 10 min and incubated with 1:200 biotinylated goat anti-rabbit antibody (Dakocytomation) for 1 hr at room temperature. After two PBST washes (for 10 min each), the sections were incubated in a 1:8000 Streptavidin-FluoProbe SR 101 (Interchim; Montluçon, France) in the dark at room temperature. After two PBST washes (for 5 min each), the sections were mounted in a fluorescent-free aqueous mountant glycerol/PBS (9/1, v/v). Image acquisition was immediately carried out with a fluorescent microscope (Axiophot II; Zeiss, Jena, Germany) equipped with a motorized XY stage and a cooled AxioCam HRc CCD camera (Zeiss) controlled by the Axiovision 4.4 digital image processing software. The Mark and Find module of this software was used to record the various positions photographed on the slides. Thereafter, the coverslips were removed, and the sections were soaked in 0.1 N HCl for 20 min to eliminate the tissue-bound antibodies. After two PBST washes (for 5 min each), the second immunostaining sequence was carried out following the steps used in the first sequence. The antisera to active caspase-7 and c-PARP were respectively applied at a 1:50 and 1:25 dilution, and in the third step, Streptavidin Fluo Probe Alexa 488 (Interchim; Montluçon, France), diluted 1:4000, was used in place of Streptavidin-FluoProbe SR 101. The Mark and Find module was used to relocate the fields previously recorded, which were again photographed at the same magnification. The images of the same fields recorded under the two fluorescent modalities were merged using Axiovision software. Several controls were performed. First, the absence of cross-reactivity caused by residual antibodies of the first step was checked by omitting the second primary antibody of the double immunostaining method. Second, the absence of the deleterious effect of HCl on the second antibody signal was verified.

Statistical Analysis

Mann-Whitney's *U*-test was used to determine the statistical significance, with a limit set to $p<0.05$ using Staview 5.0 software.

Results

Apoptosis and Apoptosis-related Protein Assessment in Monolayer Cell Pellets

Morphological and IHC aspect of apoptosis was studied in three monolayer cell lines after their pretreat-

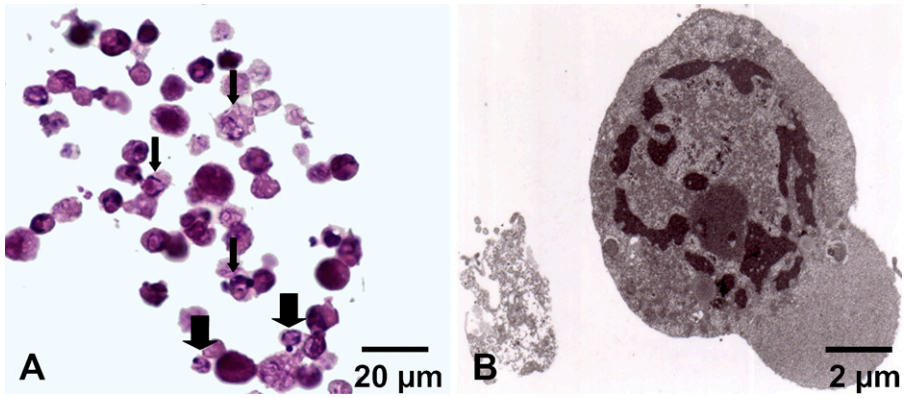

Figure 2 Apoptosis in MDA-MB231 monolayer cells subjected to Foscan-photodynamic treatment (PDT). (**A**) Paraffin sections were stained with standard coloration HES. Note specific morphological features of apoptosis such as condensed eosinophilic cytoplasm and clumped marginated chromatin (thin arrows) or apoptotic bodies (thick arrows). (**B**) Transmission electron microscopy. Ultrastructural study showed an MDA-MB231 cell with a nuclear marginated chromatin and an increase in the cytosol density typical of apoptosis.

ment with paclitaxel, an apoptosis inducer in many cell lines. Apoptosis was first recorded by morphological study on hematoxylin-eosin-safran-stained tissue sections (Figure 1A). Specific morphological changes indicative of apoptosis were identified in HT29 and KB cells but not in MDA cells (thin arrows). All cell lines, however, showed numerous cells with mitotic nuclei as a consequence of paclitaxel cytostatic treatment (thick arrows). The antibodies specific for active caspases-3 and -7 (Figures 1B and 1C) selectively stained the cytoplasm of cells (thin arrows), whose nuclear morphology was consistent with apoptosis, along with the cytoplasm of morphologically healthy-looking cells, thus suggesting that these antibodies recognized activated protein at the early stage of apoptosis. Active caspase-3, opposite to caspase-7, was also occasionally detected in nuclei (thick arrows), thus featuring a translocation of the protein to the nucleus (Figure 1B). In apoptotic cells, whose nuclei were still not fragmented, c-PARP staining was limited to nuclear chromatin (Figure 1D, thick arrows) and was distributed rather uniformly and diffusely over the whole nuclear area. Apoptotic bodies were clearly stained by all three markers.

After Foscan-PDT, a similar aspect in stained cells detected either by active caspase-3, active caspase-7, or c-PARP antibodies was obtained in HT29 and KB compared with paclitaxel treatment (data not shown). In MDA-MB231cells, typical apoptotic features including specific chromatin distribution and cytoplasm densification were observed both in HES (Figure 2A) and ultrastructural examinations (Figure 2B). The chromatin was predominantly arranged as a circumferential layer of heterochromatin, whereas the central chromatin had a dispersed granula rand speckled appearance. An increase in electron density was observed in the cytosol (Figure 2B).

Similar ultrastructural modifications were observed in other cells treated by PDT along with HT 29 and KB cells after paclitaxel treatment (data not shown).

The apoptotic indices (AIs) obtained from all three markers in HT29, KB, and MDA-MB231 cell lines are shown in Figure 3. Overall, <4% of the cells were detected by the three markers in controls. We noticed that the number of cells labeled with the antibody to c-PARP gave statistically significant lower results compared with other markers. Irrespective of cell lines, mean AIs in control were 0.47 ± 0.2% for c-PARP, 1.28 ± 1.03% for active caspase-3 (p = 0.02), and 1.19 ± 0.71% for active caspase-7 (p = 0.008). Similarly, paclitaxel-treated MDA-MB231 cells showed significantly less c-PARP–labeled cells (0.68 ± 0.30%) than active caspase-3 (1.72 ± 0.28%)– or active caspase-7 (1.79 ± 0.46%)–labeled cells (p<0.05). In paclitaxel-treated HT29 and KB cells, c-PARP labeling (22.7 ± 15.0% and 15.4 ± 5.4%, respectively) and active caspase-7 labeling (23.8 ± 19.8 and 14.3 ± 3.5%,

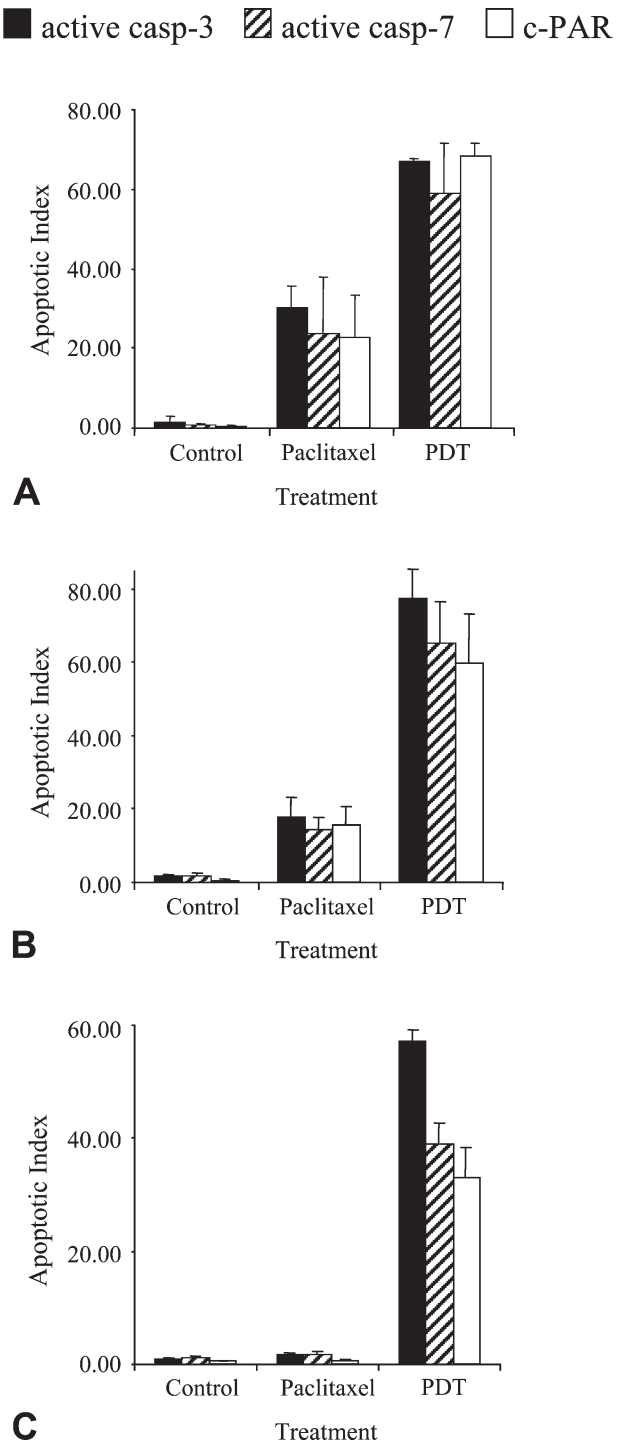

Figure 3 Apoptotic index from active caspase-3, active caspase-7, or c-PARP staining applied on control or treated HT29 (**A**), KB (**B**), and MDA-MB231 (**C**) cells. Cells were treated either by paclitaxel or Foscan-PDT. Results are expressed as mean apoptotic index (AI) ± SD of three experiments determined from at least 2000 tumor cells in each section. *Significantly different values (p<0.05).

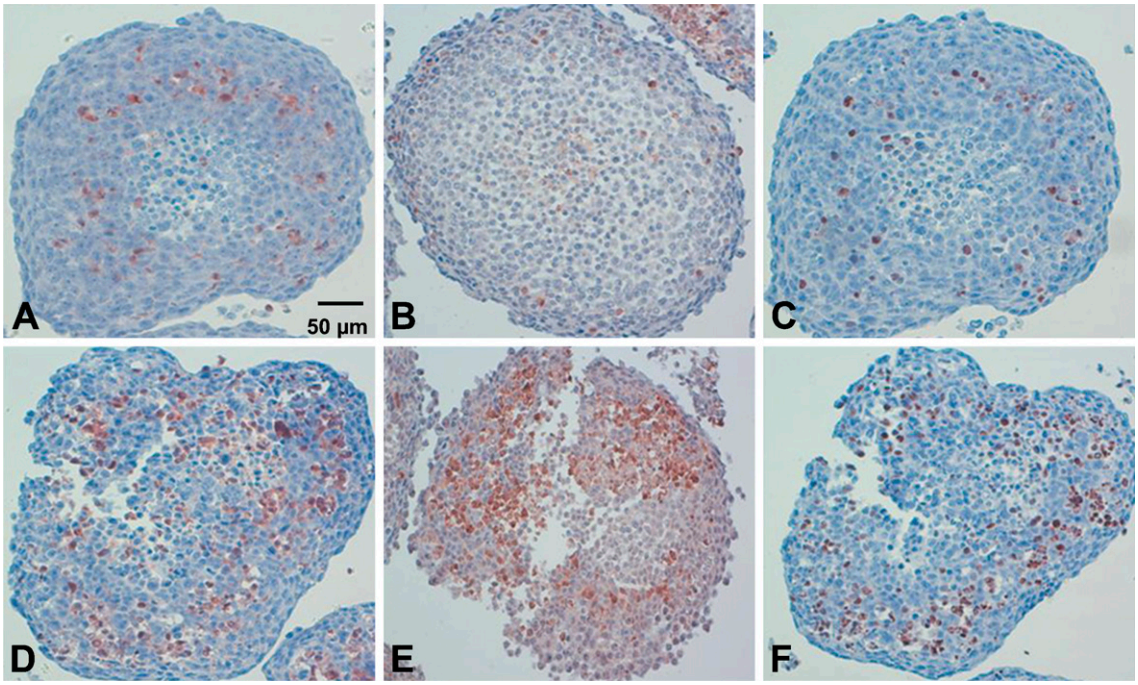

Figure 4 IHC on paraffin sections of HT29 spheroids to active caspase-3 (**A,D**), active caspase-7 (**B,E**), or c-PARP (**C,F**) applied without treatment (**A–C**) or subjected to Foscan-PDT (**D–F**). Note the distribution of apoptotic cells at the periphery of necrotic area. Loss of cell cohesion was noticeable in spheroids subjected to Foscan-PDT (**D–F**). Harris' hematoxylin counterstain.

respectively) gave close AIs, whereas active caspase-3 labeling yielded slightly but not significantly greater AIs (30.2 ± 7.6% and 17.8 ± 5.2%, respectively). In Foscan-photosensitized cells, IHC analysis to active caspase-3, caspase-7, or c-PARP did not result in a statistically significant difference in HT29 (67.1 ± 0.8%, 58.8 ± 18.2%, and 68.2 ± 4.7%, respectively) or KB cells (77.3 ± 8.2%, 65.0 ± 11.5%, and 59.6 ± 13.7%, respectively). In MDA-MB231 cells, active caspase-3 clearly provided greater AI (57.0 ± 2.1%) than either active caspase-7 (38.9 ± 3.8%) or c-PARP (32.9 ± 5.5%) labeling ($p<0.05$).

Apoptosis-related Protein Assessment in Spheroids

IHC to active caspase-3, active caspase-7, and c-PARP was applied to 29 spheroids subjected to different treatment protocols. Figure 4 shows the distribution of cells detected by the antibodies to active caspase-3, active caspase-7, and c-PARP in control spheroids (Figures 4A, 4B, and 4C, respectively) and in spheroids subjected to Foscan-PDT (Figures 4D, 4E, and 4F, respectively). Control spheroids showed a few labeled cells around the necrotic core as clearly shown in the spheroids immunostained with either antiactive caspase-3 (Figure 4A) or anti-c-PARP antibody (Figure 4C). In Foscan-photosensitized spheroids (Figures 4D–4F), the number of labeled cells increased in the area between the outer rim and the necrotic core. In addition, we noted a loss of cell cohesion. Distribution pattern of staining was the same irrespective of the technique used. AIs determined from non-necrotic cells of untreated or treated either by paclitaxel or Foscan-PDT spheroids are presented in Table 1. In control spheroids, from 9.1% to 17.3% labeled cells were counted according to the method applied, with the lowest value for c-PARP (9.1 ± 2.3%). The highest and identical scores were obtained with active caspase-3 (17.4 ± 3.0%) and active caspase-7 (17.0 ± 4.4%) labeling and were found sig-

Table 1 Quantification of apoptotic cells by IHC to c-PARP and active caspase-3 and -7 in paraffin-embedded section of control[a] and paclitaxel[b] or Foscan-photosensitized[c] HT29 spheroids

	Apoptotic index[d]		
Markers	Control cells	Paclitaxel	Foscan-PDT
Active caspase-3	17.4 ± 3.0	34.7 ± 1.9	38.4 ± 0.4
Active caspase-7	17.0 ± 4.4	32.3 ± 7.1	40.3 ± 3.8
c-PARP	9.1 ± 2.3[e]	32.4 ± 2.2	41.3 ± 0.7

[a]Control tumors were obtained from both untreated HT29 and non-irradiated cell spheroids.
[b]HT29 spheroids were incubated with 0.1 µM paclitaxel for 48 hr.
[c]HT29 spheroids were subjected to 4.5 µM Foscan for 24 hr before irradiation (10 mW/cm^2, 5 J/cm^2).
[d]Mean ± SD of at least three experiments.
[e]Significantly different ($p<0.05$).
c-PARP, cleaved poly-ADP-ribose polymerase; PDT, photodynamic treatment.

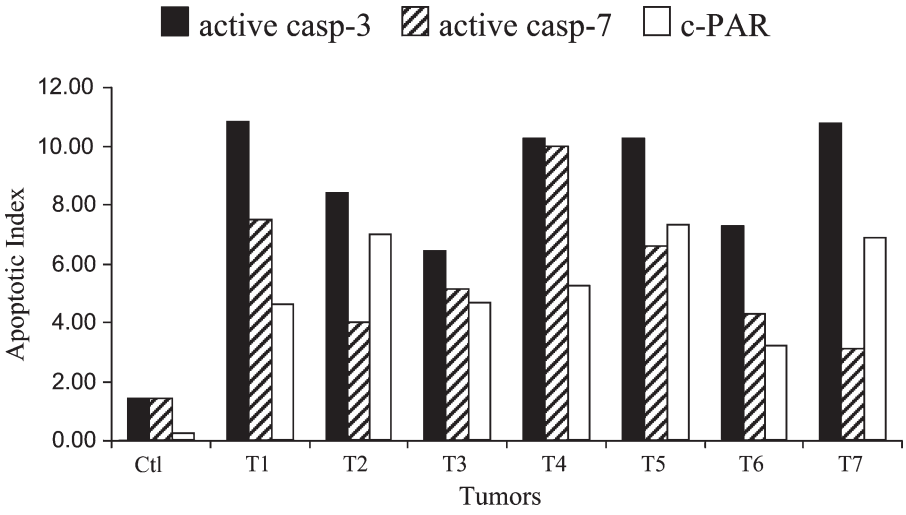

Figure 5 Apoptotic index from active caspase-3, active caspase-7, or c-PARP staining applied on HT29 subcutaneous xenografts subjected to Foscan (0.3 mg/kg, IV) photosensitization (10 J/cm^2, 30 mW/cm^2, 24 hr after injection). Note the variability between tumors. AIs were determined from at least 2000 tumor cells in each section.

nificantly different from c-PARP value ($p<0.05$). In paclitaxel-treated spheroids IHC toward active caspase-3, active caspase-7, and c-PARP resulted in equivalent AIs (34.7 ± 1.9%, 32.3 ± 7.1%, and 32.4 ± 2.2%, respectively). A similar observation was found in Foscan-photosensitized spheroids (38.4 ± 0.4%, 40.3 ± 3.8%, and 41.3 ± 0.7%, respectively).

Apoptosis-related Protein Assessment in HT29 Subcutaneous Xenografts

The density of apoptotic cells was assessed in three control tumors and in seven xenografts 24 hr after Foscan-PDT (Figure 5). Variability in the level of apoptosis was patent. Overall, the extent of apoptosis detected with c-PARP in control tumors was significantly lower (0.2 ± 0.2%) than active caspase-3 (1.4 ± 1.2%) or active caspase-7 (1.4 ± 0.7%) immunostaining ($p<0.05$). In Foscan-photosensitized tumors, active caspase-3 labeling prevailed in all cases. This observation was confirmed by the comparison of AIs averaged for each marker (Table 2). Maximal staining (8.3 ± 2.9%) was obtained for active caspase-3 and was found significantly different ($p<0.02$) from active caspase-7 (4.9 ± 1.5%) and c-PARP (5.0 ± 2.0%).

Overlaid images taken from immunofluorescence experiments performed on a tissue section subjected successively to active caspase-3 and c-PARP in control (Figure 6A) or in Foscan-photosensitized tumors (Figure 6B) provided additional information. In all labeled cells, c-PARP (shown in green) colocalized with active caspase-3 (shown in red), thus providing yellow spots. In some cases, tiny yellow spots were enclosed in red signals suggesting limited expression of c-PARP. This feature was predominantly observed in control tumors (Figure 6A). A careful examination of immunostained tissue sections (Figures 6C and 6D) confirmed this observation. Many apoptotic cells from control tumors showed nuclei containing a limited part of labeled antigenic sites (Figure 6C), whereas photosensitized tumors showed a higher number of cells with a large expression of c-PARP (Figure 6D). These cells were noticed without apoptotic-related nuclear morphological change, suggesting that apoptosis in these cells was at an early stage.

Another observation from immunofluorescence analysis was the poor correlation between active caspase-3 (red) and active caspase-7 (green) in Foscan-photosensitized tumors (Figure 7). Expression of active caspase-7 was not detectable in all active caspase-3–expressing cells. As a result, some labeled cells exhibited only a red signal. Conversely, all cells detected by the antibody to active caspase-7 expressed active caspase-3 antigen, thus showing yellow spots.

Discussion

Two major apoptotic pathways, namely the extrinsic (through membrane death receptor) and intrinsic (through mitochondria), are governed by caspases, a

Table 2 Quantification of apoptotic cells by IHC to c-PARP and active caspase-3 and -7 in paraffin-embedded section of control[a] and Foscan-photosensitized[b] HT29 xenografted tumors

	Apoptotic index[c]	
Markers	Control tumors	Foscan-PDT
Active caspase-3	1.4 ± 1.2	8.3 ± 2.9[d]
Active caspase-7	1.4 ± 0.7	4.9 ± 1.5
c-PARP	0.2 ± 0.2[d]	5.0 ± 2.0

[a]Control tumors were obtained from both untreated HT29 and non-irradiated tumors.
[b]Nude mice were injected with 0.3 mg/kg Foscan 24 hr before tumor irradiation (30 mW/cm^2, 10 J/cm^2).
[c]Mean ± SD of at least three experiments.
[d]Significantly different ($p<0.05$).
c-PARP, cleaved poly-ADP-ribose polymerase; PDT, photodynamic treatment.

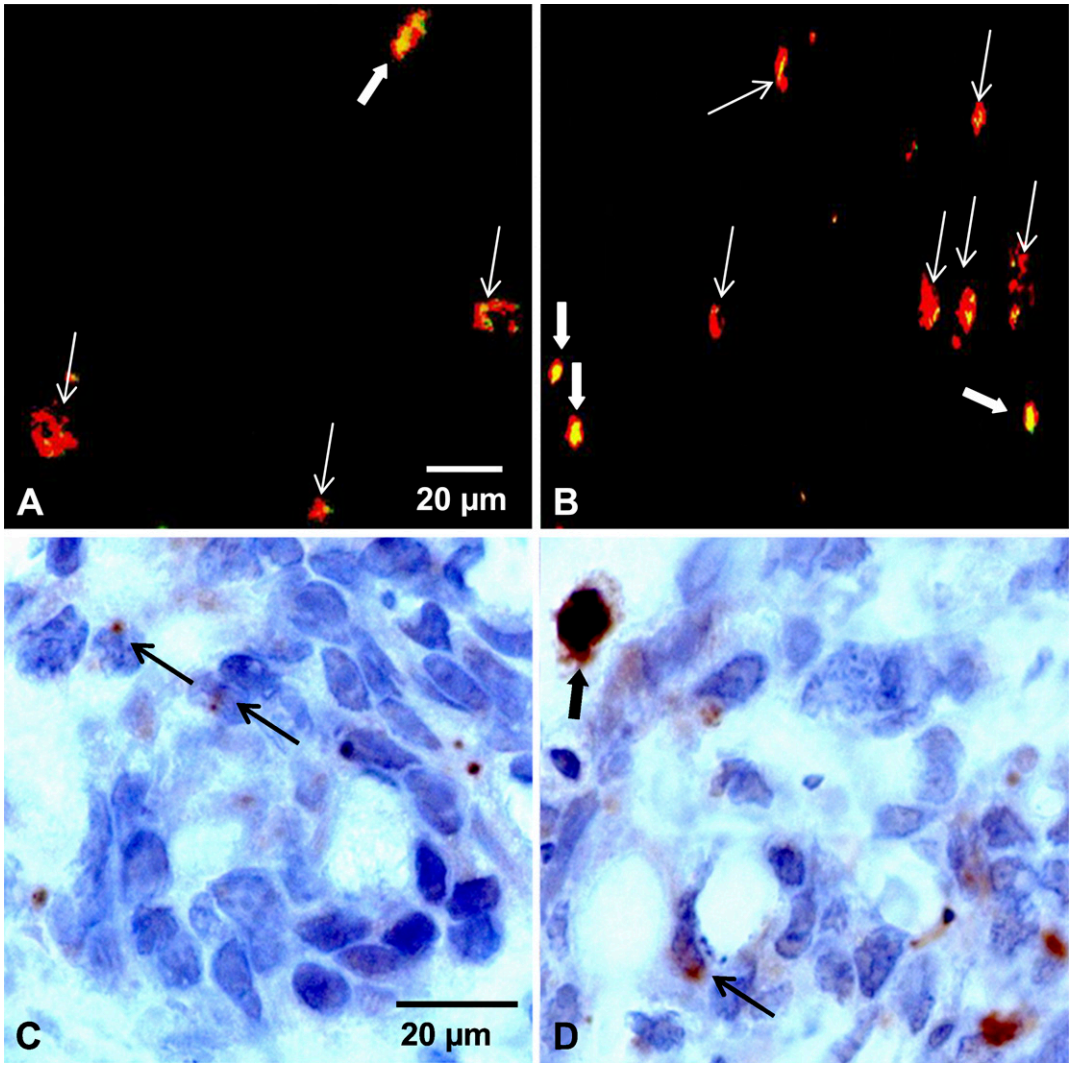

Figure 6 Merging of immunofluorescence images obtained from control tumors (**A**) or Foscan (0.3 mg/kg, IV)-photosensitized (10 J/cm^2, 30 mW/cm^2) HT29 subcutaneous xenografts (**B**) frozen 24 hr after treatment. Frozen sections were first subjected to active caspase-3 (red fluorescence) and then to c-PARP (green fluorescence). Colocalization between both markers showed large yellow spots (thick white arrows) or tiny yellow spots (thin white arrows) caused by c-PARP expression. c-PARP IHC on paraffin sections of control tumors (**C**) and photosensitized tumors (**D**). Thin black arrows indicate limited expression of c-PARP, whereas the thick black arrow indicates a large expression of c-PARP in nuclei of apoptotic cells.

family of proteases that cleave substrates at Asp-Xxx sequence. Based on their function, caspases have been divided into initiators or executioners of apoptosis. The executioner class includes caspase-3, caspase-6, which is processed by caspase-3 (Slee et al. 2001), and caspase-7. The precise role of caspase-7 during apoptosis remains elusive (Slee et al. 2001; Lakhani et al. 2006), whereas caspase-3 is generally considered to be the primary executioner of apoptosis. Therefore, the development of antibodies targeting either the active form of caspase-3 or cleaved substrates resulting from its activation warrants investigation (Holubec et al. 2005; Jakob et al. 2008).

In this study, we proposed to extend the investigation to caspase-7 processing and PARP-1 cleavage. Caspases-3 and -7 have some overlapping but also some distinct roles in apoptosis. It has been shown that caspase-3 controls DNA fragmentation and morphological changes of apoptosis (Slee et al. 2001; Lakhani et al. 2006). Caspase-7 plays a little role in these processes but could be important in the loss of cellular viability (Lakhani et al. 2006). In this context, PARP, which is generally recognized as a substrate of both caspases-3 and -7 with a strong affinity for the latter (Germain et al. 1999), could be a very useful marker of apoptosis. We performed an IHC study of apoptosis

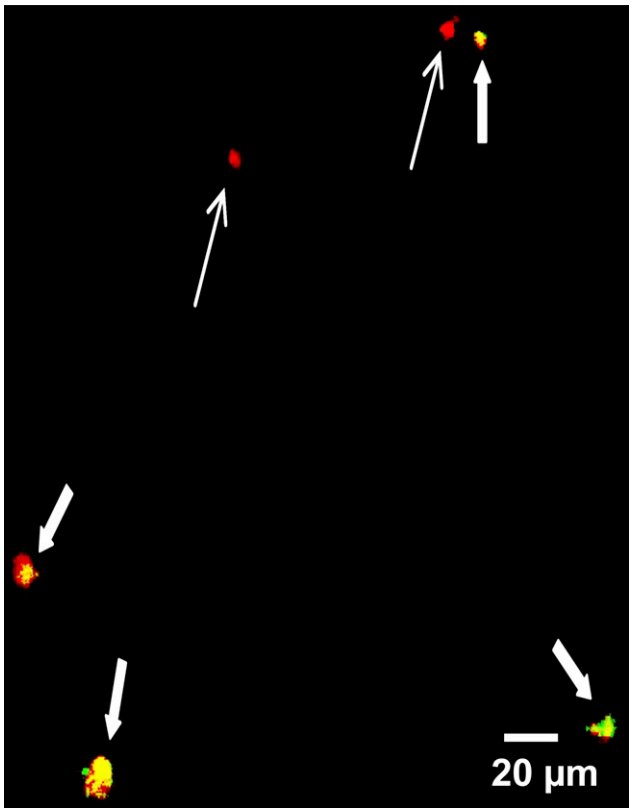

Figure 7 Merging of immunofluorescence images obtained from Foscan (0.3 mg/kg, IV)-photosensitized (10 J/cm^2, 30 mW/cm^2) HT29 subcutaneous xenografts frozen 24 hr after treatment. Frozen sections were first subjected to active caspase-3 (red fluorescence) and then to active caspase-7 (green fluorescence). Colocalization between both markers showed yellow spots (thick arrows). Red spots (thin arrows) indicate active caspase-3 expression only.

at three different levels of preclinical models, monolayer cells from three cell lines (HT29, KB, and MDA-MB231), HT29 cell spheroids that mimic avascular microtumors, and HT29 tumors xenografted in nude mice. Apoptotic cells at the late stage of the process showed morphological criteria (chromatin condensation with a marked accumulation of densely stained chromatin at the edge of the nucleus and cell fragmentation with formation of apoptotic bodies) that enabled their identification by standard hematoxylin and eosin staining. However, in paclitaxel-treated cells, abnormal mitotic figures resembling those of apoptosis could be confusing (Figure 1A). Active caspase-3 immunostaining was confirmed as a highly sensitive method that could clearly show the different steps in the location of caspase-3 activation from cytoplasmic to nuclear translocation of the protein (Figure 1B). This latter feature was not observed with active caspase-7 (Figure 1C), which does not translocate into the nucleus after induction of apoptosis (Kamada et al. 2005), thus supporting the difference between the two caspases in their respective role in the nuclear morphological changes during apoptosis. c-PARP labeling in the whole area of apoptotic nuclei (Figure 1C) was anticipated because PARP-1 is a DNA-binding enzyme that signals DNA strand breaks. Moreover, we applied an antibody to the large 85-kDa fragment of c-PARP, which has been shown to be translocated from the nucleolus to the nucleoplasm during apoptosis, whereas the short 29-kDa fragment is retained in nucleoli (Alvarez-Gonzalez et al. 1999). Compared with active caspase-3 or -7 labeling, the use of the antibody to c-PARP resulted in a poor staining of cells undergoing physiological apoptosis in control samples or in apoptosis-resistant MDA-MB231 cells treated with paclitaxel (Figure 3; Tables 1 and 2). Further analysis performed by merging the immunofluorescence images indicated a high level of colocalization between active caspase-3 and c-PARP in HT29 tumors (Figures 6A and 6B). A similar observation has been earlier reported in medulloblastomas (Puig et al. 2001). However, immunofluorescence from c-PARP labeling was restricted to tiny spots (Figure 7A), indicating a limited expression of the protein that could explain the difficulty to detect the cleaved form of PARP by enzymatic IHC. After treatment in vitro of HT29 or KB cells either by paclitaxel or by Foscan-PDT, the pattern of c-PARP labeling was close to those of active caspases-3 and -7 (Figures 3A, 3B, and 4). Likewise, in Foscan-photosensitized MDA-MB231, IHC to c-PARP and active caspase-7 resulted in a non-significantly different AI values (Figure 3C). These results suggest that cell damage either increased the number of antigenic sites and/or modified the extend of expression of c-PARP large fragments over the nucleus. In fact, both events could be related to the overactivation of full-length PARP-1 shortly before or simultaneously to the cleavage of PARP by caspases (Germain et al. 1999; Simbulan-Rosenthal et al. 1999; D'Amours et al. 2001). It has been recently reported that the nucleolus serves as a storage supplying PARP-1 in response to heavy DNA damage (Mortusewicz et al. 2007). Thus, the translocation of 85-kDa PARP fragments from the nucleolus to the nucleoplasm could occurs along with covalently bound poly(ADP-ribose) generated by the poly(ADP-ribosyl)ation catalyzed by the massive recruitment of PARP-1 from nucleoli to damage sites (Alvarez-Gonzalez et al. 1999). Taken together, these observations could imply a close relationship between the activity of PARP poly(ADP-ribosyl)ation, the amount of antigenic sites and the distribution of cleaved fragments over the nucleus after treatment. In this context, the percentage of c-PARP–labeled cells (5.0 ± 2.0%; Table 2) in Foscan-photosensitized HT29 tumors could represent an accurate evaluation of photoinduced apoptosis, whereas apoptotic assessment through caspases-3 or -7 activation includes both basic physiological and treatment-induced apoptosis.

Both treatments, paclitaxel and Foscan-PDT, trigger apoptosis in cells by the activation of caspases-3 and -7 (Goncalves et al. 2000; Kottke et al. 2002; Marchal et al. 2005). Caspase-7 has been recently presumed to play a major role in the induction of apoptosis under severe oxidative stress of the endoplasmic reticulum (Reddy et al. 2003; Rao et al. 2004). This molecular pathway has been strongly suggested after Foscan-PDT in the mammary adenocarcinoma MCF-7 cell line that lacks caspase-3 (Marchal et al. 2007). IHC to active caspase-3 and active caspase-7 applied on HT29 and KB monolayer cells and HT29 spheroids treated by either paclitaxel or Foscan-PDT showed a close percentage of cells expressing caspase-3 or caspase-7 activation (Figures 3A and 3B; Table 1). Thus, equal involvement of both caspases in the apoptotic pathway may be presumed. On the other hand, in Foscan-photosensitized MDA-MB231 cells (Figure 3C) or HT29 tumors (Table 2), active caspase-3 labeling was predominant. Colocalization obtained from merged immunofluorescence images indicated that active caspase-7 was not expressed in all caspase-3–expressing cells (Figure 7), suggesting that Foscan-PDT–induced apoptosis was mainly processed through the activation of caspase-3 in HT29 tumors. Likewise, MDA-MB231 monolayer cells could be more susceptible to caspase-3 activation after Foscan-PDT than HT29 and KB cell lines.

In conclusion, the use of c-PARP as a marker of physiological apoptosis is doubtful, whereas it could be a useful indicator of treatment-induced apoptosis probably by DNA damage. The biological significance in the different pattern of expression of active caspase-3 and -7 in Foscan-photosensitized tumors needs further study. As a general rule, the use of different antibodies to differentiate caspase-dependent apoptotic pathways in vivo is relevant.

Acknowledgments

We thank Biolitec AG for providing the Foscan.

Literature Cited

Alvarez-Gonzalez R, Spring H, Muller M, Burkle A (1999) Selective loss of poly(ADP-ribose) and the 85-kDa fragment of poly(ADP-ribose) polymerase in nucleoli during alkylation-induced apoptosis of HeLa cells. J Biol Chem 274:32122–32126

Coutier S, Bezdetnaya LN, Foster TH, Parache RM, Guillemin F (2002) Effect of irradiation fluence rate on the efficacy of photodynamic therapy and tumor oxygenation in meta-tetra (hydroxyphenyl) chlorin (mTHPC)-sensitized HT29 xenografts in nude mice. Radiat Res 158:339–345

D'Amours D, Sallmann FR, Dixit VM, Poirier GG (2001) Gain-of-function of poly(ADP-ribose) polymerase-1 upon cleavage by apoptotic proteases: implications for apoptosis. J Cell Sci 114: 3771–3778

Davidson DJ, Haskell C, Majest S, Kherzai A, Egan DA, Walter KA, Schneider A, et al. (2005) Kringle 5 of human plasminogen induces apoptosis of endothelial and tumor cells through surface-expressed glucose-regulated protein 78. Cancer Res 65: 4663–4672

Decker P, Muller S (2002) Modulating poly (ADP-ribose) polymerase activity: potential for the prevention and therapy of pathogenic situations involving DNA damage and oxidative stress. Curr Pharm Biotechnol 3:275–283

Degterev A, Boyce M, Yuan J (2003) A decade of caspases. Oncogene 22:8543–8567

Duan WR, Garner DS, Williams SD, Funckes-Shippy CL, Spath IS, Blomme EA (2003) Comparison of immunohistochemistry for activated caspase-3 and cleaved cytokeratin 18 with the TUNEL method for quantification of apoptosis in histological sections of PC-3 subcutaneous xenografts. J Pathol 199:221–228

Germain M, Affar EB, D'Amours D, Dixit VM, Salvesen GS, Poirier GG (1999) Cleavage of automodified poly(ADP-ribose) polymerase during apoptosis. Evidence for involvement of caspase-7. J Biol Chem 274:28379–28384

Goncalves A, Braguer D, Carles G, Andre N, Prevot C, Briand C (2000) Caspase-8 activation independent of CD95/CD95-L interaction during paclitaxel-induced apoptosis in human colon cancer cells (HT29–D4). Biochem Pharmacol 60:1579–1584

Gown AM, Willingham MC (2002) Improved detection of apoptotic cells in archival paraffin sections: immunohistochemistry using antibodies to cleaved caspase 3. J Histochem Cytochem 50: 449–454

Green DR, Kroemer G (2004) The pathophysiology of mitochondrial cell death. Science 305:626–629

Holubec H, Payne CM, Bernstein H, Dvorakova K, Bernstein C, Waltmire CN, Warneke JA, et al. (2005) Assessment of apoptosis by immunohistochemical markers compared to cellular morphology in ex vivo-stressed colonic mucosa. J Histochem Cytochem 53:229–235

Jakob S, Corazza N, Diamantis E, Kappeler A, Brunner T (2008) Detection of apoptosis in vivo using antibodies against caspase-induced neo-epitopes. Methods 44:255–261

Jin Z, El-Deiry WS (2005) Overview of cell death signaling pathways. Cancer Biol Ther 4:139–163

Kamada S, Kikkawa U, Tsujimoto Y, Hunter T (2005) Nuclear translocation of caspase-3 is dependent on its proteolytic activation and recognition of a substrate-like protein(s). J Biol Chem 280: 857–860

Koh DW, Dawson TM, Dawson VL (2005) Mediation of cell death by poly(ADP-ribose) polymerase-1. Pharmacol Res 52:5–14

Kottke TJ, Blajeski AL, Meng XW, Svingen PA, Ruchaud S, Mesner PW Jr, Boerner SA, et al. (2002) Lack of correlation between caspase activation and caspase activity assays in paclitaxel-treated MCF-7 breast cancer cells. J Biol Chem 277:804–815

Lakhani SA, Masud A, Kuida K, Porter GA Jr, Booth CJ, Mehal WZ, Inayat I, et al. (2006) Caspases 3 and 7: key mediators of mitochondrial events of apoptosis. Science 311:847–851

Marchal S, Fadloun A, Maugain E, D'Hallewin MA, Guillemin F, Bezdetnaya L (2005) Necrotic and apoptotic features of cell death in response to Foscan photosensitization of HT29 monolayer and multicell spheroids. Biochem Pharmacol 69:1167–1176

Marchal S, Francois A, Dumas D, Guillemin F, Bezdetnaya L (2007) Relationship between subcellular localisation of Foscan and caspase activation in photosensitised MCF-7 cells. Br J Cancer 96:944–951

McGrogan BT, Gilmartin B, Carney DN, McCann A (2008) Taxanes, microtubules and chemoresistant breast cancer. Biochim Biophys Acta 1785:96–132

Miller JD, Baron ED, Scull H, Hsia A, Berlin JC, McCormick T, Colussi V, et al. (2007) Photodynamic therapy with the phthalocyanine photosensitizer Pc 4: the case experience with preclinical mechanistic and early clinical-translational studies. Toxicol Appl Pharmacol 224:290–299

Mooney LM, Al-Sakkaf KA, Brown BL, Dobson PR (2002) Apoptotic mechanisms in T47D and MCF-7 human breast cancer cells. Br J Cancer 87:909–917

Mortusewicz O, Ame JC, Schreiber V, Leonhardt H (2007) Feedback-regulated poly(ADP-ribosyl)ation by PARP-1 is required for rapid

response to DNA damage in living cells. Nucleic Acids Res 35: 7665–7675

Puig B, Tortosa A, Ferrer I (2001) Cleaved caspase-3, caspase-7 and poly (ADP-ribose) polymerase are complementarily but differentially expressed in human medulloblastomas. Neurosci Lett 306:85–88

Pyrko P, Schonthal AH, Hofman FM, Chen TC, Lee AS (2007) The unfolded protein response regulator GRP78/BiP as a novel target for increasing chemosensitivity in malignant gliomas. Cancer Res 67:9809–9816

Rao RV, Ellerby HM, Bredesen DE (2004) Coupling endoplasmic reticulum stress to the cell death program. Cell Death Differ 11: 372–380

Reddy RK, Mao C, Baumeister P, Austin RC, Kaufman RJ, Lee AS (2003) Endoplasmic reticulum chaperone protein GRP78 protects cells from apoptosis induced by topoisomerase inhibitors: role of ATP binding site in suppression of caspase-7 activation. J Biol Chem 278:20915–20924

Resendes AR, Majo N, Segales J, Espadamala J, Mateu E, Chianini F, Nofrarias M, et al. (2004) Apoptosis in normal lymphoid organs from healthy normal, conventional pigs at different ages detected by TUNEL and cleaved caspase-3 immunohistochemistry in paraffin-embedded tissues. Vet Immunol Immunopathol 99: 203–213

Simbulan-Rosenthal CM, Rosenthal DS, Iyer S, Boulares H, Smulson ME (1999) Involvement of PARP and poly(ADP-ribosyl)ation in the early stages of apoptosis and DNA replication. Mol Cell Biochem 193:137–148

Slee EA, Adrain C, Martin SJ (2001) Executioner caspase-3, -6, and -7 perform distinct, non-redundant roles during the demolition phase of apoptosis. J Biol Chem 276:7320–7326

The Journal of Histochemistry & Cytochemistry